

X-RAY INSIGHTS INTO THE NATURE OF WEAK EMISSION-LINE QUASARS AT HIGH REDSHIFT

OHAD SHEMMER,^{1,2} W. N. BRANDT,¹ SCOTT F. ANDERSON,³ ALEKSANDAR M. DIAMOND-STANIC,⁴ XIAOHUI FAN,⁴
GORDON T. RICHARDS,⁵ DONALD P. SCHNEIDER,¹ AND MICHAEL A. STRAUSS⁶

Received 2008 September 3; accepted 2009 January 28

ABSTRACT

We present *Chandra* observations of nine high-redshift quasars ($z = 2.7 - 5.9$) discovered by the Sloan Digital Sky Survey with weak or undetectable high-ionization emission lines in their UV spectra (WLQs). Adding archival X-ray observations of six additional sources of this class has enabled us to place the strongest constraints yet on the X-ray properties of this remarkable class of AGNs. Although our data cannot rule out the possibility that the emission lines are overwhelmed by a relativistically boosted continuum, as manifested by BL Lac objects, we find that WLQs are considerably weaker in the X-ray and radio bands than the majority of BL Lacs found at much lower redshifts. If WLQs are high-redshift BL Lacs, then it is difficult to explain the lack of a large parent population of X-ray and radio bright weak-lined sources at high redshift. We also consider the possibility that WLQs are quasars with extreme properties, and in particular that the emission lines are suppressed by high accretion rates. Using joint spectral fitting of the X-ray spectra of 11 WLQs we find that the mean photon index in the hard X-ray band is consistent with those observed in typical radio-quiet AGNs with no hint of an unusually steep hard-X-ray spectrum. This result poses a challenge to the hypothesis that WLQs have extremely high accretion rates, and we discuss additional observations required to test this idea.

Subject headings: galaxies: active – galaxies: nuclei – X-rays: galaxies – quasars: general – quasars: emission lines

1. INTRODUCTION

Since strong and broad emission lines are a hallmark of quasar optical–UV spectra, the discovery of ~ 50 Sloan Digital Sky Survey (SDSS; York et al. 2000) quasars at $z \sim 2.7 - 5.9$ with extremely weak or undetectable emission lines (hereafter WLQs) is puzzling (see Fan et al. 1999 for the discovery of the prototype high-redshift WLQ, SDSS J153259.96–003944.1, at $z = 4.62$). While the rest-frame equivalent widths (EWs) of the $\text{Ly}\alpha + \text{N V}$ emission lines of typical SDSS quasars at $z \sim 3$ follow a log-normal distribution and 68% of EWs are in the range $\sim 40 - 100 \text{ \AA}$ (Fan et al. 2001; Diamond-Stanic et al. 2009), WLQs exhibit $\text{EW}(\text{Ly}\alpha + \text{N V}) < 10 \text{ \AA}$, constituting a 4σ deviation from the mean of the distribution (there is no detectable corresponding deviation at the high EW end; Diamond-Stanic et al. 2009). By virtue of their largely featureless spectra, the redshifts of these WLQs can be determined only from the onset of the $\text{Ly}\alpha$ forest or the Lyman limit (i.e., $z > 2.2$ for SDSS sources; e.g., Fan et al. 1999; Anderson et al. 2001; Collinge et al. 2005; Schneider et al. 2005).

Since WLQs exhibit typical quasar UV continua with no signs of broad C IV absorption, they are unlikely to be dust-obscured or broad-absorption line quasars (see, e.g., Anderson et al. 2001; Collinge et al. 2005). In addition, Shemmer et al. (2006; hereafter S06) have argued against the possibility that these sources are high-redshift galaxies with appar-

ent quasar-like luminosities due to gravitational-lensing amplification, or lensed quasars with continua amplified by microlensing. S06 suggested that the two most likely interpretations for the weakness of the high-ionization emission lines in these sources are either line dilution due to a relativistically boosted continuum or, alternatively, physical suppression of the high-ionization emission lines.

The first interpretation for the nature of WLQs involves relativistic beaming of the continuum emission from a jet directed close to our line of sight, as observed in BL Lacertae objects (BL Lacs). This scenario implies that the SDSS may have discovered the long-sought, high-redshift BL Lacs (e.g., Stocke 2001); the absence of such sources is even more puzzling since their beamed continua should have made them easier to detect at high redshift than ordinary quasars. However, this interpretation faces serious difficulties. For example, S06 have found that the basic X-ray, optical, and radio properties of five WLQs are consistent only with the X-ray- and radio-weak tail of the BL Lac population. Moreover, while both WLQs and BL Lacs share the property of a lineless UV spectrum, BL Lacs also often exhibit high optical polarization levels, rapid and large-amplitude flux variations, and spectral energy distributions (SEDs) dominated by beamed, non-thermal emission at all wavelengths (e.g., Urry & Padovani 1995). Such extreme properties have, so far, not been observed in a subsample of SDSS WLQs (e.g., Fan et al. 1999; Diamond-Stanic et al. 2009).

The alternative interpretation is that WLQs may be quasars with abnormal photoionizing continuum or broad emission-line region (BELR) properties. In this scenario, the weak high-ionization emission lines of WLQs may, for example, ultimately be a consequence of exceptionally high accretion rates in these sources. A higher accretion rate is expected to result in a softer, UV-peaked continuum that suppresses the high-ionization emission lines, while low-ionization species such as the Balmer and Fe II lines are not significantly affected (e.g., Leighly et al. 2007a,b). Accretion rates in WLQs

¹ Department of Astronomy & Astrophysics, The Pennsylvania State University, University Park, PA 16802

² Current address: Department of Physics, University of North Texas, Denton, TX 76203; ohad@unt.edu

³ Department of Astronomy, University of Washington, Box 351580, Seattle, WA 98195

⁴ Steward Observatory, University of Arizona, 933 North Cherry Avenue, Tucson, AZ 85721

⁵ Department of Physics, Drexel University, 3141 Chestnut Street, Philadelphia, PA 19104

⁶ Princeton University Observatory, Peyton Hall, Princeton, NJ 08544

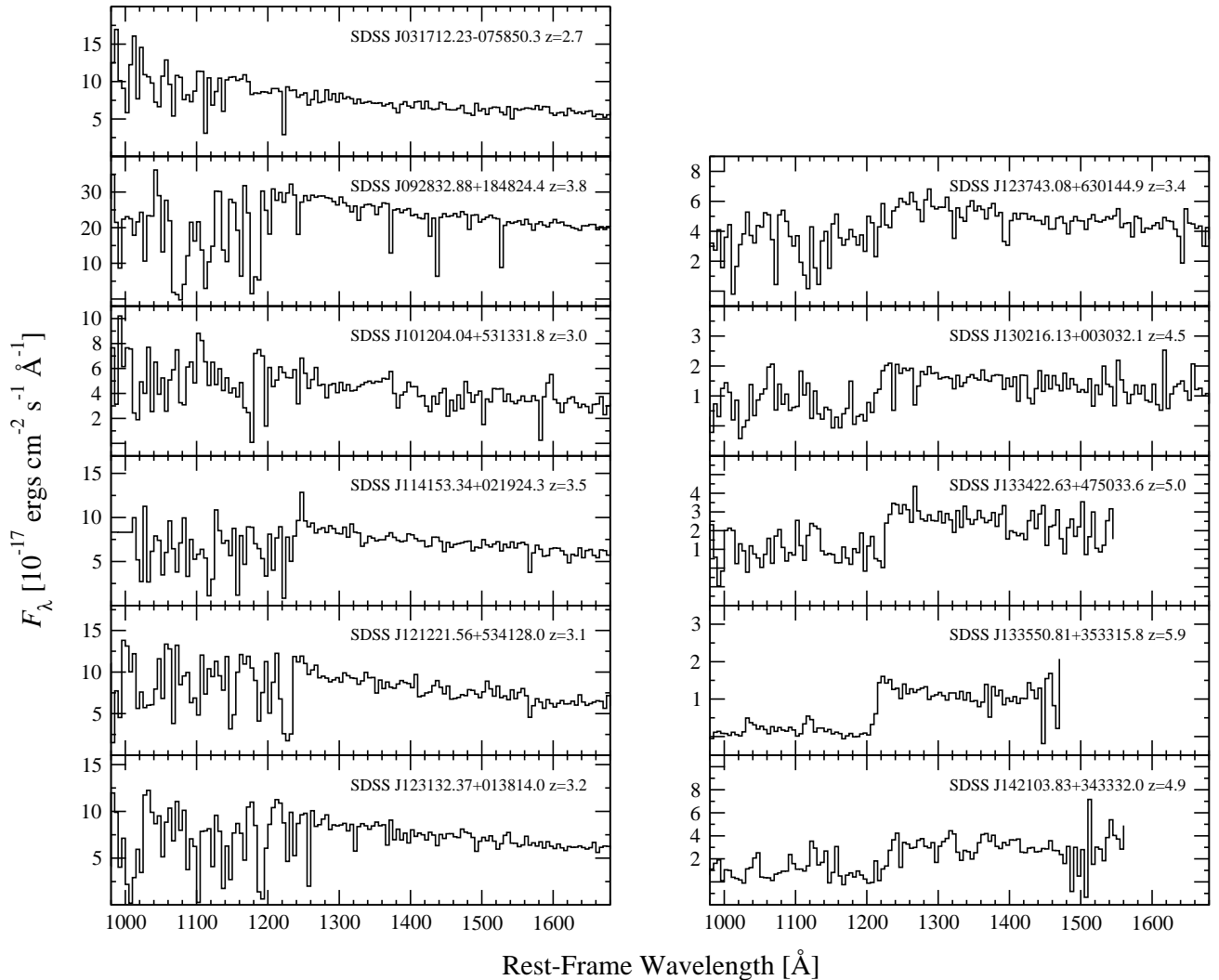


FIG. 1.— Ultraviolet spectra of the WLQ sample resampled in bins of 5 \AA , for clarity. Spectra were obtained from the SDSS archive, except for SDSS J1335+3533, for which the spectrum was obtained from the Keck observatory (Fan et al. 2006).

have not yet been determined in order to test this possibility (for example, by measuring the width of $H\beta$ in such sources; see, e.g., Shemmer et al. 2004).

The key to understanding WLQs, therefore, lies in comparing their multiwavelength spectral, as well as polarimetric and temporal, properties with those of BL Lacs and typical quasars. While the SDSS WLQs are rare, their exceptional properties constitute a challenge to our overall understanding of AGN physics and thus might lead to new insights about the accretion process, emission-line formation, and relativistic jets. In this paper, we measure basic X-ray properties for the first respectably sized sample of WLQs in order to shed light on their nature and to assist in planning more detailed X-ray spectroscopy of these sources in the future. Since X-rays probe the innermost regions of AGNs, our observations are intended to study the basic diagnostics of the central accretion process in WLQs. This paper nearly triples the number of $z > 2.2$ WLQs that have sensitive X-ray coverage, increasing the number of X-ray detections by almost a factor of five.

This paper is organized as follows: in § 2 we describe the WLQ sample selection, as well as our X-ray observations and their reduction; our basic findings are presented in § 3. In § 4 we discuss the main results emerging from our X-ray study

of WLQs and the clues they provide on the nature of these sources; a summary is given in § 5. Complete WLQ names are given in the tables and figures, and their abbreviated versions are used throughout the text. Throughout this work we compute luminosity distances using the standard cosmological model with parameters $H_0 = 70 \text{ km s}^{-1} \text{ Mpc}^{-1}$, $\Omega_\Lambda = 0.7$, and $\Omega_M = 0.3$.

2. SAMPLE SELECTION, OBSERVATIONS, AND DATA REDUCTION

2.1. Targeted Chandra observations

We selected nine WLQs at $z = 2.7 - 5.9$ for short ($\sim 4 - 23 \text{ ks}$) *Chandra* observations in Cycle 8 (2007–2008); the rest-frame ultraviolet spectra of these sources appear in Fig. 1. The *Chandra* observation log appears in Table 1, where we also list the papers in which the sources were first identified as WLQs or BL Lac candidates. These sources were selected from the SDSS archive for being the brightest sources of this class; except for SDSS J1302+0030, these were not targeted in X-rays prior to Cycle 8. SDSS J1302+0030 was not detected in a 10.81 ks *Chandra* Cycle 4 exposure; our additional 10.50 ks exposure in Cycle 8 has enabled its detection (see below). SDSS J1335+3533 was discovered by Fan

TABLE 1
Chandra OBSERVATION LOG

Object (SDSS J)	z	$\Delta_{\text{Opt-X}}^{\text{a}}$ (arcsec)	X-ray Obs. Date	<i>Chandra</i> Obs. ID	Exp. Time ^b (ks)	Ref.
031712.23–075850.3	2.7	0.1	2007 Mar 17	7780	4.42	1
092832.90+184824.4	3.8	0.1	2007 Jan 2	7779	3.98	2
114153.34+021924.3	3.5	0.2	2007 Feb 10	7777	3.99	1
121221.56+534128.0	3.1	0.4	2007 Jul 24	7778	4.13	1
123132.38+013814.0	3.2	0.1	2007 Jul 5	7781	4.09	1
130216.13+003032.1 ^c	4.5	0.6 ^d	2007 Feb 24	7784	10.50	3
133422.63+475033.6	5.0	0.1	2007 Aug 25	7885	11.60	3
133550.81+353315.8	5.9	0.2	2008 Mar 10	7783	23.47	4
142103.83+343332.0	4.9	0.3	2008 Feb 27	7782	12.79	5

REFERENCES. — (1) Collinge et al. (2005); (2) this work; (3) Schneider et al. (2005); (4) Fan et al. (2006); (5) Schneider et al. (2007).

NOTE. — The optical positions of the quasars have been obtained from the reference given in the seventh column, and the X-ray positions have been obtained with WAVDETECT.

^a Angular distance between the optical and X-ray positions.

^b The *Chandra* exposure time has been corrected for detector dead time.

^c A 10.81 ks *Chandra* Cycle 4 exposure of the source (Obs. ID 3958) is not reflected in this Table. The Cycle 8 observation raises the total exposure time on the source to 21.31 ks, and the merged event file is used in subsequent analyses throughout the paper (see S06 and § 2 for details).

^d Based on a merged image composed of *Chandra* Cycle 4 and Cycle 8 exposures.

et al. (2006) and is the only source in this sample that was not detected with the SDSS quasar-selection algorithm (Richards et al. 2002; this algorithm is not designed to detect quasars above $z \simeq 5.4$).

The nine WLQs were observed with the Advanced CCD Imaging Spectrometer (ACIS; Garmire et al. 2003) with the S3 CCD at the aimpoint. Faint mode was used for the event telemetry format in all the observations, and ASCA grade 0, 2, 3, 4, and 6 events were used in the analysis, which was carried out using standard CIAO⁷ v3.4 routines. No background flares are present in these observations. Source detection was carried out with WAVDETECT (Freeman et al. 2002) using wavelet transforms (with wavelet scale sizes of 1, 1.4, 2, 2.8, and 4 pixels) and a false-positive probability threshold of 10^{-4} . Given the small number of pixels being searched due to the accurate a priori source positions and the subarcsecond on-axis angular resolution of *Chandra*, the probability of spurious detections is extremely low; most of the sources were in fact detected at a false-positive probability threshold of 10^{-6} . The X-ray positions of the detected sources differ by $0.1''$ – $0.6''$ from their optical positions (Table 1). These results are consistent with expected *Chandra* positional errors.

The X-ray counts detected in the ultrasoft band (0.3–0.5 keV), soft band (0.5–2 keV), hard band (2–8 keV), and full band (0.5–8 keV) are reported in Table 2. The counts were derived from manual aperture photometry, and they are consistent with the photometry obtained using WAVDETECT. Except for SDSS J1302+0030, all of the targeted WLQs were detected with 3–110 full-band counts. A significant detection of SDSS J1302+0030 (using WAVDETECT with a false-positive probability threshold of 10^{-4}) was achieved only by merging the Cycle 8 exposure (with 3 full-band counts) with that from Cycle 4 (with 2 full-band counts; see S06); the X-ray counts for this source, presented in Table 2, were obtained from the merged image. Table 2 also includes the band ratio, which is the ratio between the counts in the hard band and the counts in the soft band, and the effective

power-law photon index [Γ , where $N(E) \propto E^{-\Gamma}$; Γ was calculated from the band ratio using the *Chandra* PIMMS v3.9d tool⁸] for each source.

Finally, we searched for rapid variability within the *Chandra* observations of all WLQs detected with > 10 full-band counts by applying a Kolmogorov-Smirnov (KS) test to the photon arrival times against the null hypothesis of a constant rate, but no significant flux variations were detected. This result is not unexpected given the combination of the relatively short observations (15–30 min in the rest-frame) and the small number of detected photons from most of the sources.

2.2. Serendipitous XMM-Newton observations

Two additional SDSS WLQs at $z > 2.2$ were serendipitously observed by *XMM-Newton* (Jansen et al. 2001). SDSS J1012+5313 at $z = 3.0$ is a newly identified WLQ from SDSS Data Release 5 (Schneider et al. 2007). The source was observed with *XMM-Newton* on 2001 April 19 for 18.7 ks (dataset ID 0111100201; PI M. Watson). SDSS J1237+6301 at $z = 3.4$ was identified as a BL Lac candidate by Collinge et al. (2005). The source was observed with *XMM-Newton* on 2006 October 25 for 20.7 ks (dataset ID 0402250101; PI B. Maughan). The *XMM-Newton* observations were processed using standard *XMM-Newton* Science Analysis System⁹ v7.1.0 tasks. The SDSS J1012+5313 observation included only MOS1 and MOS2 images, and the entire observation was carried out during a period of flaring activity; hence no time filtering was employed. The SDSS J1237+6301 observation was filtered in time to remove periods of background flaring in which the count rates of each MOS (pn) detector exceeded 0.35 (1.0) counts s^{-1} for events having $E > 10$ keV; the net exposure times were 10.7 ks and 4.9 ks for the MOS1/MOS2 and pn detectors, respectively. We detected SDSS J1012+5313 at $7.0'$ from the *XMM-Newton* aimpoint in both the MOS1 and MOS2 detectors. For each detector, source counts were extracted from an aperture with a $30''$ radius centered on the source, and background counts were ex-

⁷ *Chandra* Interactive Analysis of Observations.
<http://cxc.harvard.edu/ciao/>

⁸ <http://cxc.harvard.edu/toolkit/pimms.jsp>

⁹ <http://xmm.esac.esa.int/sas>

TABLE 2
X-RAY COUNTS, BAND RATIOS, AND EFFECTIVE PHOTON INDICES

Object (SDSS J)	X-ray Counts ^a				Band Ratio ^b	Γ^b
	0.3–0.5 keV	0.5–2 keV	2–8 keV	0.5–8 keV		
031712.23–075850.3	< 3.0	23.9 ^{+6.0} _{-4.8}	3.0 ^{+2.9} _{-1.6}	26.8 ^{+6.3} _{-5.1}	0.13 ^{+0.13} _{-0.07}	2.6 ^{+0.8} _{-0.6}
092832.90+184824.4	< 3.0	52.2 ^{+8.3} _{-7.2}	10.9 ^{+4.4} _{-3.2}	63.1 ^{+9.0} _{-7.9}	0.21 ^{+0.09} _{-0.07}	2.2 ^{+0.4} _{-0.3}
114153.34+021924.3	< 4.8	28.6 ^{+6.4} _{-5.3}	12.7 ^{+4.7} _{-3.5}	41.4 ^{+7.5} _{-6.4}	0.44 ^{+0.19} _{-0.15}	1.4 ^{+0.4} _{-0.3}
121221.56+534128.0	< 3.0	3.0 ^{+2.9} _{-1.6}	< 3.0	3.0 ^{+2.9} _{-1.6}	< 1.00	> 0.7
123132.38+013814.0	10.9 ^{+4.4} _{-3.2}	83.6 ^{+10.2} _{-9.1}	26.5 ^{+6.2} _{-5.1}	109.9 ^{+11.5} _{-10.4}	0.32 ^{+0.08} _{-0.07}	1.7 ^{+0.2} _{-0.2}
130216.13+003032.1 ^c	< 3.0	2.0 ^{+2.7} _{-1.3}	< 8.0	5.0 ^{+3.4} _{-2.2}	< 4.00	> -0.6
133422.63+475033.6	< 4.8	13.8 ^{+4.8} _{-3.7}	4.0 ^{+3.2} _{-1.9}	17.7 ^{+5.3} _{-4.2}	0.29 ^{+0.25} _{-0.16}	1.8 ^{+0.7} _{-0.6}
133550.81+353315.8	< 3.0	3.0 ^{+2.9} _{-1.6}	< 6.4	5.0 ^{+3.4} _{-2.2}	< 2.13	> 0.0
142103.83+343332.0	< 3.0	2.0 ^{+2.7} _{-1.3}	< 4.8	3.8 ^{+3.1} _{-1.9}	< 2.40	> -0.1

^a Errors on the X-ray counts were computed according to Tables 1 and 2 of Gehrels (1986) and correspond to the 1σ level; these were calculated using Poisson statistics. The upper limits are at the 95% confidence level and were computed according to Kraft, Burrows, & Nousek (1991). Upper limits of 3.0, 4.8, 6.4, and 8.0 indicate that 0, 1, 2, and 3 X-ray counts, respectively, have been found within an extraction region of radius $1''$ centered on the optical position of the quasar (considering the background within this source-extraction region to be negligible).

^b We calculated errors at the 1σ level for the band ratio (the ratio between the 2–8 keV and 0.5–2 keV counts) and effective photon index following the “numerical method” described in § 1.7.3 of Lyons (1991); this avoids the failure of the standard approximate-variance formula when the number of counts is small (see § 2.4.5 of Eadie et al. 1971). The photon indices have been obtained applying the correction required to account for the ACIS quantum-efficiency decay at low energy.

^c The X-ray counts, band ratio, and photon index for this source were obtained from a merged event file of our new *Chandra* Cycle 8 observation and an archival *Chandra* Cycle 4 observation (see § 2 for more details). The total exposure time of the merged event file is 21.31 ks.

tracted from an aperture with a similar size in a nearby source-free region. SDSS J1237+6301 was not detected in any of the *XMM-Newton* detectors. The upper limit on the X-ray flux of the source was taken as the square root of the number of counts encircled within an aperture of $30''$ centered on the optical position of the source (which is offset by $9.8'$ from the aimpoint) multiplied by three (i.e., a 3σ upper limit). The X-ray counts of SDSS J1012+5313 as well as the upper limit on the number of counts of SDSS J1237+6301 were corrected for vignetting using the exposure maps due to the large offsets from the aimpoints. The SDSS spectra of the two sources appear in Figure 1.

3. RESULTS

3.1. Basic Multiwavelength Properties of the WLQ Sample

Table 3 (placed at the end of the paper) lists the basic X-ray, optical, and radio properties of our WLQ sample:

Column (1). — The SDSS J2000.0 quasar coordinates, accurate to $\sim 0.1''$ (Pier et al. 2003).

Column (2). — The Galactic column density in units of 10^{20} cm^{-2} , taken from Dickey & Lockman (1990) and obtained with the HEASARC N_{H} tool.¹⁰

Column (3). — The monochromatic AB magnitude at a rest-frame wavelength of 1450 \AA ($AB_{1450} = -2.5 \log f_{1450 \text{ \AA}} - 48.6$; Oke & Gunn 1983). All the magnitudes have been corrected for Galactic extinction (Schlegel, Finkbeiner, & Davis 1998). Except for SDSS J1335+3533, for which this magnitude has been obtained from a Keck spectrum, all the magnitudes were obtained from SDSS Data Release 5 spectra and a fiber light-loss correction has been applied; this was calculated as the difference between the synthetic i magnitude (i.e., the integrated flux across the i bandpass in the SDSS spectrum)

and the photometric SDSS i magnitude, assuming no flux variation between the photometric and spectroscopic epochs. *Column (4)*. — The absolute B -band magnitude, computed assuming a UV–optical ($\sim 1200 - 4000 \text{ \AA}$) power-law slope of $\alpha_{\text{UV}} = -0.5$ ($f_{\nu} \propto \nu^{\alpha_{\text{UV}}}$; Vanden Berk et al. 2001).

Columns (5) and (6). — The flux density and monochromatic luminosity at a rest-frame wavelength of 2500 \AA , computed from the magnitudes in Col. 3, assuming a UV–optical power-law slope as in Col. 4.

Columns (7) and (8). — The count rate in the observed-frame 0.5–2 keV band and the corresponding flux, corrected for Galactic absorption. The fluxes have been calculated using PIMMS, assuming a power-law model with $\Gamma = 2.0$.

Columns (9) and (10). — The flux density and monochromatic luminosity at a rest-frame energy of 2 keV, computed assuming $\Gamma = 2.0$ in the entire *Chandra* band (0.5–8 keV).

Column (11). — The luminosity in the rest-frame 2–10 keV band.

Column (12). — The optical-to-X-ray power-law slope, α_{ox} , defined as:

$$\alpha_{\text{ox}} = \frac{\log(f_{2 \text{ keV}}/f_{2500 \text{ \AA}})}{\log(\nu_{2 \text{ keV}}/\nu_{2500 \text{ \AA}})} \quad (1)$$

where $f_{2 \text{ keV}}$ and $f_{2500 \text{ \AA}}$ are the flux densities at rest-frame 2 keV and 2500 \AA , respectively.

Column (13). — The difference between the measured α_{ox} (from Col. 12) and the predicted α_{ox} , given the UV luminosity from Col. 6, based on the observed $\alpha_{\text{ox}}-L_{\nu}(2500 \text{ \AA})$ relation in AGNs (given as Eq. 3 of Just et al. 2007; see also Steffen et al. 2006). The statistical significance of this difference is also given in units of σ , where $\sigma = 0.146$ for $31 < \log L_{\nu}(2500 \text{ \AA}) < 32$, and $\sigma = 0.131$ for $32 < \log L_{\nu}(2500 \text{ \AA}) < 33$ (see Table 5 of Steffen et al. 2006; these differences do not account for flux-density measurement errors).

¹⁰ <http://heasarc.gsfc.nasa.gov/cgi-bin/Tools/w3nh/w3nh.pl>

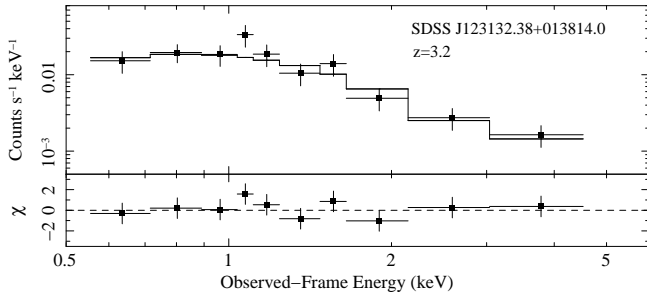


FIG. 2.— *Chandra* spectrum of SDSS J1231+0138. Filled squares represent the binned spectrum, and the solid histogram represents the best-fit Galactic-absorbed power-law model. The χ residuals are in units of σ with error bars of size 1.

Column (14). — The radio-to-optical power-law slope, α_{ro} , defined as:

$$\alpha_{ro} = \frac{\log(f_5 \text{ GHz}/f_{2500 \text{ \AA}})}{\log(\nu_5 \text{ GHz}/\nu_{2500 \text{ \AA}})} \quad (2)$$

This parameter can be directly converted to the radio-loudness parameter R (where $R = f_5 \text{ GHz}/f_{4400 \text{ \AA}}$; Kellermann et al. 1989) in the following way:

$$\alpha_{ro} = \frac{\log \left[R \left(\frac{2500}{4400} \right)^{\alpha_{UV}} \right]}{\log(\nu_5 \text{ GHz}/\nu_{2500 \text{ \AA}})} \quad (3)$$

where we take $\alpha_{UV} = -0.5$ (as in Col. 4). The flux density at a rest-frame frequency of 5 GHz was computed from the FIRST (Becker, White, & Helfand 1995) flux density at an observed-frame frequency of 1.4 GHz, if available. Otherwise, the NVSS (Condon et al. 1998) flux density at the same observed band was used. We assume a radio power-law slope of $\alpha_r = -0.5$ ($f_\nu \propto \nu^{\alpha_r}$; e.g., Rector et al. 2000). Upper limits on α_{ro} are at the 3σ level, since the positions of all our sources are known a priori. The flux densities at rest frame 4400 Å were computed from the AB_{1450} magnitudes assuming $\alpha_{UV} = -0.5$ (as in Col. 4). Typical α_{ro} values are < -0.39 (i.e., $R > 100$) for radio-loud quasars (RLQs) and > -0.21 (i.e., $R < 10$) for radio-quiet quasars (RQQs). Seven of our sources are RQQs; four sources are radio intermediate with $-0.39 \lesssim \alpha_{ro} \lesssim -0.21$ (i.e., $10 \lesssim R \lesssim 100$).

3.2. The X-ray Spectrum of SDSS J1231+0138

SDSS J1231+0138 is the only WLQ in our sample with sufficient X-ray counts to allow an investigation of its X-ray spectrum. The spectrum of the source was extracted with the CIAO task PSEXTRACT using a circular region of $2''$ radius centered on the X-ray centroid. The background was extracted from a source-free annulus with inner and outer radii of $5''$ and $25''$, respectively. The spectrum was binned in groups of 10 counts per bin. We used XSPEC v11.3.2 (Arnaud 1996) to fit the spectrum with a power-law model and a Galactic-absorption component, which was kept fixed during the fit ($N_H = 1.81 \times 10^{20} \text{ cm}^{-2}$; Dickey & Lockman 1990). The spectrum and its best-fit model and residuals appear in Fig. 2. The best-fit photon index is $\Gamma = 1.76^{+0.35}_{-0.34}$ with $\chi^2 = 5.57$ for 8 degrees of freedom; this photon index is consistent with the value obtained from the band ratio (Table 2) and is typical for radio-intermediate AGNs such as SDSS J1231+0138 ($\alpha_{ro} = -0.32$; see § 3.1; e.g., Reeves & Turner 2000). Adding an intrinsic-absorption component at the redshift of the source did not improve the fit; the upper

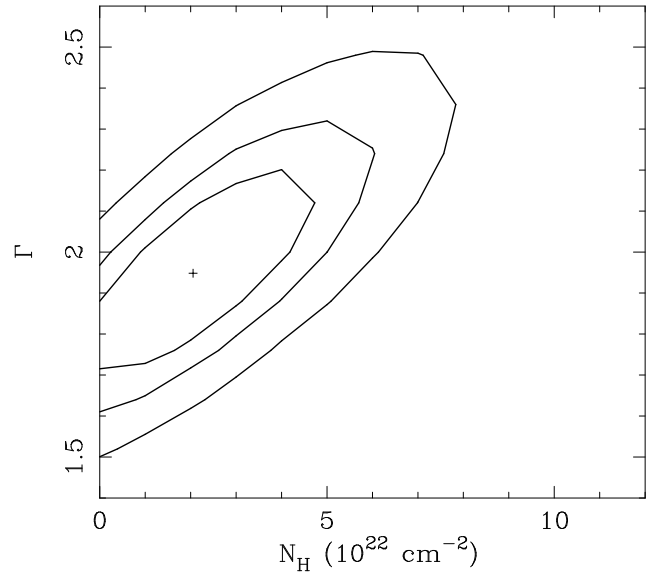


FIG. 3.— 68%, 90%, and 99% confidence regions for the photon index vs. intrinsic column density derived from joint spectral fitting of our sample of 11 WLQs over their entire observed energy range.

limit on the intrinsic absorption is $N_H \lesssim 5.70 \times 10^{22} \text{ cm}^{-2}$ (at 90% confidence).

3.3. Mean X-ray Spectral Properties of High-Redshift WLQs

Since all of our WLQs, except for SDSS J1231+0138 (see § 3.2), lack sufficient X-ray counts for individual spectral analyses, we have obtained mean X-ray spectral constraints for high-redshift WLQs as a group by jointly fitting their X-ray spectra (e.g., Vignali et al. 2005; S06). Eleven sources with *Chandra* spectra were included in the joint-fitting process, including the nine WLQs targeted in this work (i.e., all sources from Tables 1 and 2 including the merged dataset of SDSS J1302+0030) and the only other two *Chandra*-detected WLQs from S06, namely SDSS J140850.91+020522.7 and SDSS J144231.72+011055.2 (see Tables 1–3 of S06). The combined spectrum consists of a total of 350 full-band counts, obtained in 107 ks. We note that there are only two other X-ray-detected WLQs with *XMM-Newton* spectra: SDSS J1012+5313 (see § 2.2) and SDSS J004054.65–091526.8 (S06); these spectra do not provide a significant contribution to the spectral constraints since the first was taken during a period of flaring activity (§ 2.2) and the second was detected at low signal-to-noise (with only 31.8 ± 11.6 net source counts; Schneider et al. 2003).

The X-ray spectra of all 11 WLQs were extracted as in § 3.2 with PSEXTRACT using circular regions of $2''$ radius centered on the X-ray centroid of each source, and background counts were extracted using annuli of different sizes (to avoid contamination from nearby X-ray sources) centered on each source. We used XSPEC to fit the set of 11 unbinned spectra jointly with the following models: (i) a power-law model and a Galactic-absorption component (Dickey & Lockman 1990; using the PHABS absorption model in XSPEC), which was kept fixed during the fit, and (ii) a model similar to the first with an added intrinsic (redshifted) neutral-absorption component (using the ZPHABS model in XSPEC). We used the C -statistic (Cash 1979) in all the fits. The joint-fitting process associated with each quasar its own Galactic-absorption column density and redshift, and allowed the flux normalizations to

TABLE 4
BEST-FIT PARAMETERS FROM JOINT FITTING OF HIGH-REDSHIFT WLQS

XSPEC Model	Sources Included	Intrinsic N_{H} (10^{22} cm^{-2})	Γ	C-statistic (bins)
PHABS+POW	all (11 sources)	...	$1.79^{+0.17}_{-0.16}$	191.4 (294)
PHABS+POW, common energy range ^a	all (11 sources)	...	$1.96^{+0.22}_{-0.22}$	170.4 (260)
PHABS+POW	all but SDSS J1231+0138	...	$1.79^{+0.22}_{-0.22}$	133.0 (214)
PHABS+POW	seven radio-quiet WLQs ^b	...	$1.81^{+0.45}_{-0.43}$	48.2 (84)
PHABS+ZPHABS+POW	all (11 sources)	≤ 5.08	$1.95^{+0.29}_{-0.28}$	189.9 (294)
PHABS+ZPHABS+POW, common energy range ^a	all (11 sources)	≤ 4.34	$1.96^{+0.26}_{-0.22}$	170.4 (260)
PHABS+ZPHABS+POW	all but SDSS J1231+0138	≤ 7.05	$1.97^{+0.37}_{-0.35}$	131.8 (214)
PHABS+ZPHABS+POW	seven radio-quiet WLQs ^b	≤ 7.74	$1.86^{+0.72}_{-0.48}$	48.2 (84)

^a The fitting was performed only for the common rest-frame energy range among all sources (3.45–29.60 keV).

^b Excluding the radio-intermediate WLQs SDSS J0928+1848, SDSS J1141+0219, SDSS J1231+0138, and SDSS J144231.72+011055.2.

vary freely while maintaining a fixed value of the power-law photon index. The errors associated with the best-fit X-ray spectral parameters are quoted at the 90% confidence level for one parameter of interest ($\Delta C = 2.71$; Avni 1976; Cash 1979).

The joint-fitting process was carried out four times for both models. In the first run, we included the entire observed-energy range of all the spectra (0.5–8 keV). In the second run, we included only the common rest-frame energy range of all 11 sources: $3.45 \lesssim E_{\text{rest}} \lesssim 29.60$ keV (this range is based upon the entire 0.5–8 keV observed-frame band for each source, and is a consequence of the wide range of redshifts among the sources; see also S06). In the third run, we fitted the entire observed-energy range of ten WLQs, excluding SDSS J1231+0138 (since this source contributes $\sim 30\%$ of the total counts and hence might bias the results). In the fourth run, we have restricted the fitting only to radio-quiet WLQs (i.e., excluding SDSS J0928+1848, SDSS J1141+0219, SDSS J1231+0138, and SDSS J144231.72+011055.2) to minimize potential contribution from jet-related emission.

Table 4 lists the best-fit parameters from the joint-fitting process, and a contour plot of the Γ - N_{H} parameter space for the first run is shown in Figure 3. Based on F -tests, we find that the inclusion of an intrinsic-absorption component (in addition to a Galactic absorbed power-law model) does not significantly improve any of the fits; hence no significant intrinsic absorption is detected in any of the joint fits. Table 4 shows the mean photon index of WLQs is not significantly different from typical values for RQQs or radio-intermediate AGNs (e.g., Reeves & Turner 2000; Page et al. 2005; Vignali et al. 2005). In particular, there is no hint of an exceptionally high photon index as might have been expected if WLQs are high accretion-rate sources (see §4.2). The hard-X-ray spectra of AGN can appear flattened if Compton reflection is not taken into account in the spectral fitting. Since the fractional contribution from Compton reflection generally weakens with increasing luminosity, we do not expect that the typical value we obtain for the mean photon index of our luminous, high-redshift WLQs is strongly affected by Compton reflection (e.g., Iwasawa & Taniguchi 1993; Zhou & Wang 2005; Bianchi et al. 2007; Shemmer et al. 2008).

The exclusion of SDSS J1231+0138 or the exclusion of all radio-intermediate sources have no significant effect on the results (see also §3.2). In addition, photon indices derived in individual runs are consistent with each other, within the errors; these errors are large due to the limited number of sources in our sample and the short exposures. We con-

clude that the mean X-ray spectral properties of high-redshift WLQs are consistent with those observed in typical, radio-quiet-to-intermediate AGNs.

4. DISCUSSION

Our primary goal is to use X-ray information to shed light on the nature of WLQs at high redshift. The *Chandra* and serendipitous *XMM-Newton* observations have provided significantly stronger constraints on the X-ray luminosities of our WLQs than previous *ROSAT* observations (see also Collinge et al. 2005; S06). This should allow us to scrutinize the classification of the WLQs and determine the most probable explanation for the absence of their high-ionization lines. The two most likely scenarios for the absence of the UV lines are the association of WLQs with BL Lac objects or the hypothesis that WLQs are quasars with extreme properties (see §1; S06). Given the X-ray, optical, and radio luminosities presented in this work for an extended sample of 15 high-redshift WLQs (i.e., including 11 sources from this work and four sources from S06), we are now in a position to perform meaningful comparisons of these basic properties with those of BL Lacs.

4.1. Comparing WLQs with BL Lacs

For the purpose of comparing our WLQs to BL Lac objects, we have compiled a dataset of X-ray, optical, and radio luminosities for a sample of 279 BL Lacs from a variety of surveys, covering most of the current BL Lac selection methods (see, e.g., Perlman et al. 2001). We selected only BL Lacs with reliable redshifts from the *Einstein* Slew survey (11 sources; e.g., Perlman et al. 1996), the *Einstein* Medium Sensitivity Survey (EMSS; 24 sources; e.g., Rector et al. 2000), the *ROSAT* All-Sky Survey-Green Bank (RGB) catalog (47 sources; e.g., Laurent-Muehleisen et al. 1999), the Deep X-ray Radio Blazar Survey (DXRBS; 16 sources; Perlman et al. 1998; Landt et al. 2001), and the SDSS (181 sources; Collinge et al. 2005; Plotkin et al. 2008). Most BL Lacs with reliable redshifts from the 1 Jy survey (e.g., Stickel et al. 1991), i.e., radio-selected BL Lacs, overlap with sources detected in the above surveys and are included in our sample. Basic X-ray, optical, and radio properties of our BL Lac sample are given in Table 5 (placed at the end of the paper).

All fluxes and K -corrections for our BL Lac sample were computed assuming the spectral slopes $\alpha_x = -1$, $\alpha_o = -0.5$, and $\alpha_r = -0.5$ (where $f_\nu \propto \nu^\alpha$) for the X-ray, optical-UV, and radio bands, respectively; the same as those assumed for our WLQs. These spectral slopes are consistent with

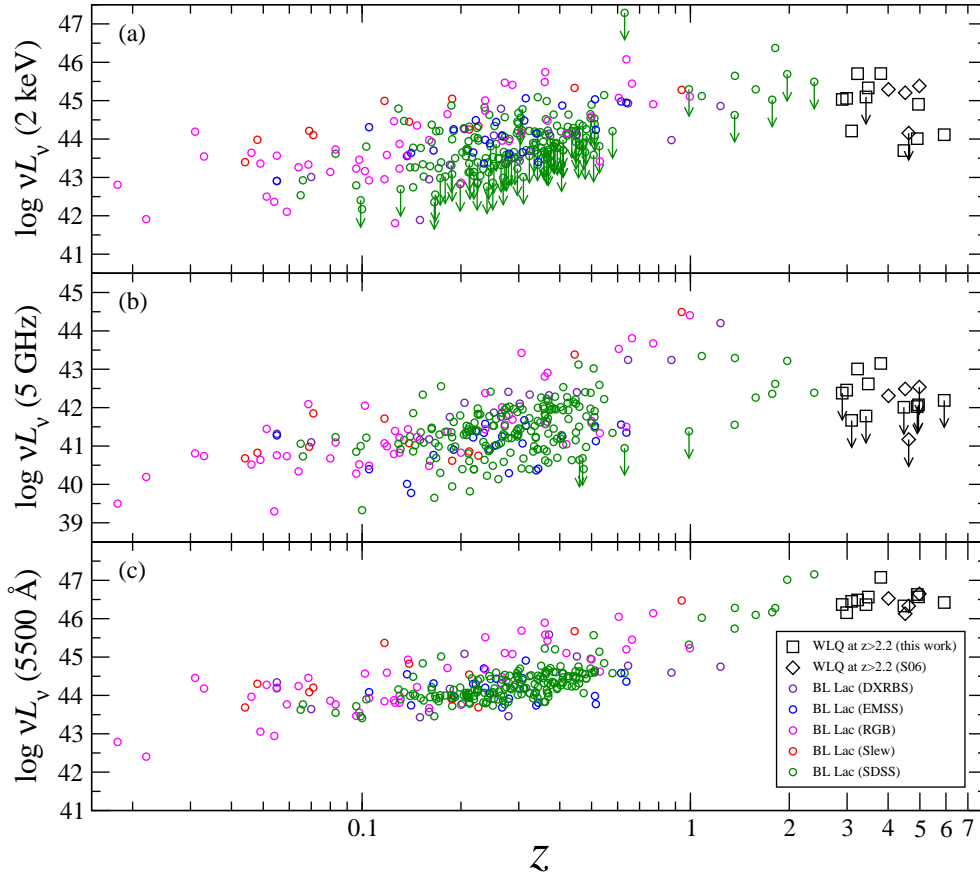


FIG. 4.— Monochromatic luminosities (in units of ergs s^{-1}) in the X-ray (a), radio (b), and optical (c) bands versus redshift for BL Lacs and WLQs. Squares mark $z > 2.2$ WLQs from this work, and diamonds mark $z > 2.2$ WLQs from S06. Violet, blue, magenta, and red circles mark BL Lacs from the DXRBS (Perلمان et al. 1998; Landt et al. 2001), EMSS (e.g., Rector et al. 2000), RGB (e.g., Laurent-Muehleisen et al. 1999), and the *Einstein Slew* (e.g., Perلمان et al. 1996) surveys, respectively. Green circles mark higher confidence SDSS BL Lac candidates with reliable redshifts from the SDSS (Collinge et al. 2005; Plotkin et al. 2008). Upper limits are marked with down-pointing arrows.

the observed values in the majority of quasars, although in the optical and radio bands they are somewhat different from the slopes observed in typical BL Lacs (e.g., Sambruna et al. 1996; Rector et al. 2000; Reeves & Turner 2000; Vanden Berk et al. 2001; Collinge et al. 2005). We repeated the optical and radio flux and K -correction calculations for the BL Lacs, this time assuming typical observed BL Lac slopes (i.e., $\alpha_r = 0.27$; e.g., Stickel et al. 1991; $\alpha_o = -1.5$; e.g., Collinge et al. 2005), and found that the differences in optical and radio fluxes between the two sets of calculations were small (since the majority of these BL Lacs lie at $z \lesssim 0.3$). In any case, the differences in optical and radio fluxes between the calculations using different slopes are well within the uncertainties stemming from measurement errors, BL Lac variability, and beaming (note that, for consistent comparisons with the observed properties of the WLQs, we make no attempt to correct the fluxes or luminosities of the BL Lacs for the effects of relativistic beaming).

In Figure 4 we present X-ray, optical, and radio monochromatic luminosities versus redshift for our BL Lac comparison sample and our extended sample of 15 WLQs. In spite of the large difference in redshift between the majority of BL Lacs ($z \lesssim 0.3$) and WLQs ($z \gtrsim 2.2$), the WLQs do not have luminosities that are so high that they are disjoint from those of the BL Lacs; a few BL Lacs even reach the optical luminosities of WLQs. The fact that no BL Lacs have been found in the redshift range of our WLQs is not yet understood (e.g., Stocke

& Perrenod 1981; Stocke 2001; Padovani et al. 2007).

Are WLQs simply the long-sought high-redshift BL Lacs? In this scenario, it is difficult to explain why there are essentially no X-ray- and/or radio-bright WLQs in Figure 5, where we have plotted α_{ox} and α_{ro} for the BL Lacs and our WLQs in a ‘color-color’ diagram (the definitions of α_{ox} and α_{ro} in § 3.1 are identical to the definitions used in S06, and note that the similar Fig. 8 of S06 included many flat-spectrum radio sources and sources with unreliable redshifts). In other words, if the SDSS high-redshift WLQs are indeed the high-redshift tail of the BL Lac population with α_{ox} and α_{ro} distributions similar to their low-redshift counterparts, then a much larger, ‘parent’ population of X-ray- and radio-bright lineless sources at high redshift is still missing. Unless these are too optically faint (see below), the SDSS, for example, should have naturally discovered many such sources had they existed (see, e.g., Collinge et al. 2005; Anderson et al. 2007; Plotkin et al. 2008). Alternatively, if most BL Lacs at low redshift were X-ray and radio weak, and thus were largely missed by X-ray and radio surveys, the SDSS should have discovered many members of this population as well (e.g., Collinge et al. 2005).

To test whether X-ray- and radio-bright BL Lacs are simply too faint and thus miss detection at high redshift, we looked for correlations between luminosity and α_{ox} and α_{ro} among our BL Lac sample. We found that α_{ox} and α_{ro} are not significantly correlated with optical luminosity. On the other hand, α_{ox} (α_{ro}) is significantly correlated with X-ray (radio) lumi-

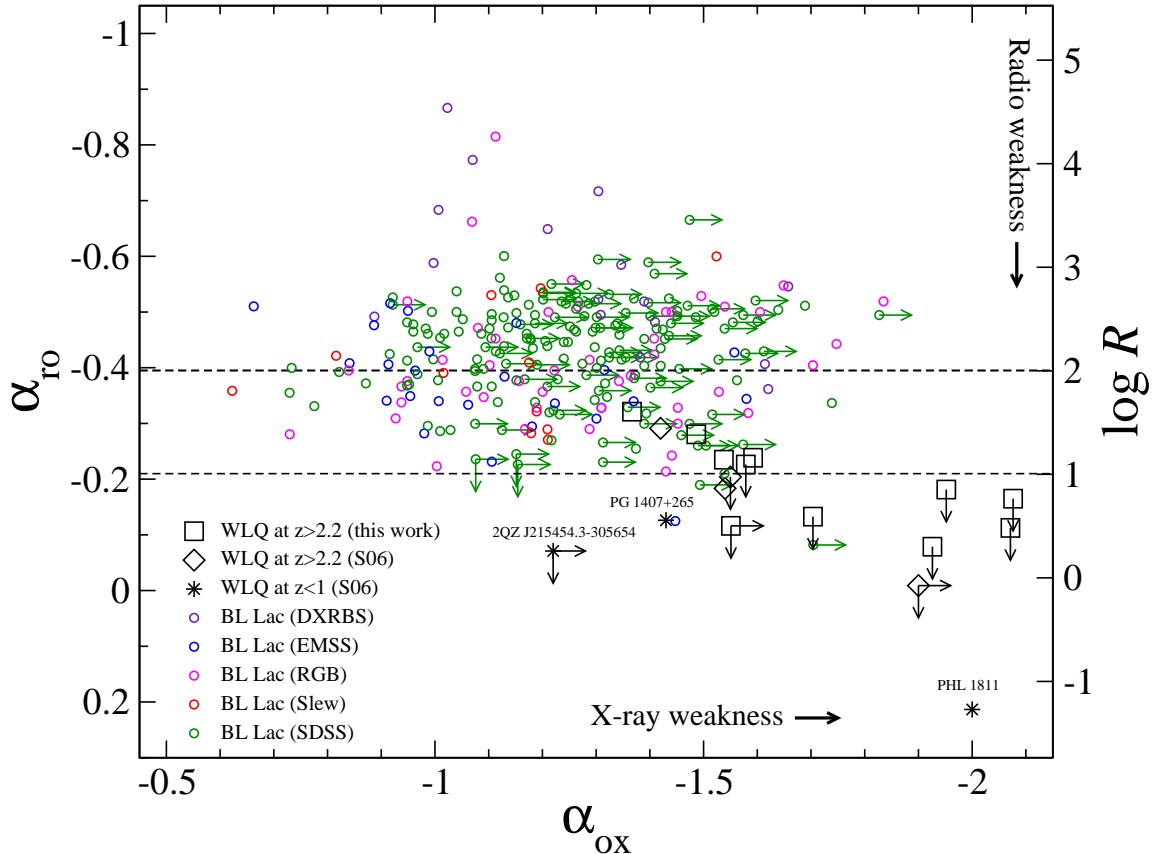


FIG. 5.— The $\alpha_{\text{ox}}-\alpha_{\text{ro}}$ diagram for BL Lacs and WLQs. Symbols are similar to those in Fig. 4. WLQs at $z < 1$ from S06 are marked with asterisks. Right (down) pointing arrows mark α_{ox} (α_{ro}) upper limits. All sources that lie above (below) the upper (lower) dashed line are radio loud (quiet) with $R > 100$ ($R < 10$).

nosity in the sense that, sources that are more X-ray (radio) luminous are also X-ray (radio) brighter relative to their optical luminosities. These results suggest that we are not missing a putative, large parent population of BL Lacs at high redshift purely due to a luminosity effect. An additional difficulty in associating WLQs with BL Lacs arises from the fact that, while there appears to be a trend of a positive X-ray-radio dependence among WLQs, there is no corresponding trend between the X-ray and radio emission of BL Lacs (i.e., for a given α_{ox} value, a BL Lac can have a wide range of α_{ro} values and vice versa; Fig. 5; see also Plotkin et al. 2008).

Are WLQs related to the rare population of radio-weak BL Lacs (see, e.g., Collinge et al. 2005; Anderson et al. 2007)? Four BL Lacs from our comparison sample, SDSS J095125.90+504559.7 at $z = 1.363$, SDSS J094602.21+274407.0 at $z = 2.382$, SDSS J145326.52+545322.4 at $z = 0.100$ (Plotkin et al. 2008), and MS 2306.1–2236 at $z = 0.137$ (Rector et al. 2000) have $\alpha_{\text{ro}} > -0.2$ and satisfy the radio-weak BL Lac (as well as radio-quiet AGN) classification; see also Table 5 of Collinge et al. (2005) for additional possible candidates from this group. Based on its redshift and UV properties, SDSS J094602.21+274407.0 may be classified as a high-

redshift WLQ (it is the radio-weakest source with an α_{ox} upper limit from the SDSS BL Lac sample in Fig. 5); we plot its SDSS spectrum in Figure 6. Further testing the association of WLQs with radio-weak BL Lacs requires broader spectroscopic coverage of both classes. For example, near-IR spectra of WLQs should be acquired to search for low-ionization emission lines in the rest-frame UV–optical band, and UV spectra of low-redshift, radio-weak BL Lacs should be obtained to measure the strengths of high-ionization emission lines. However, such observations will not resolve the missing parent population of ‘typical’ (i.e., X-ray- and radio-bright) BL Lacs at high redshift, which remains an outstanding problem for any model attempting to unify WLQs and BL Lacs.

4.2. Are WLQs Extreme Quasars?

The second scenario attempting to explain the missing UV lines in WLQs suggests that these sources are quasars hosting abnormal BELRs or quasars with extreme properties (§1). In this case, one does not expect to find many radio-bright (i.e., radio-loud) WLQs, since the majority of quasars at all luminosities and redshifts are known to be radio quiet (e.g., Jiang et al. 2007). Hence, unless emission-

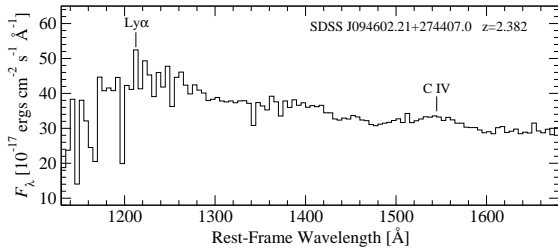


FIG. 6.— The SDSS spectrum of the BL Lac candidate SDSS J094602.21+274407.0 from Plotkin et al. (2008), which may also be classified as a WLQ. The spectrum has been resampled in bins of 5 \AA (as in Fig. 1). The locations of two prominent UV emission lines have been marked.

line strength was correlated with radio properties, there is no problem of a missing parent population (see § 4.1). In addition, the WLQs in our sample show blue UV continua with an average slope $\alpha_{UV} = -0.8$, consistent with the slopes observed for high-redshift quasars (e.g., Schneider et al. 2001) as well as with the slopes of a larger sample of high-redshift WLQs (Diamond-Stanic et al. 2009). This apparently steeper slope (compared with $\alpha_{UV} = -0.5$ observed for low-redshift quasars) is essentially due to the restricted wavelength range over which this slope can be measured in the optical spectra of high-redshift sources (i.e., given a sufficiently broad wavelength range, the UV continuum slope is $\alpha_{UV} = -0.5$, and it does not evolve with redshift; see, e.g., Schneider et al. 2005). BL Lacs, on the other hand, are considerably redder in this band (with $\alpha_o \approx -1.5$; e.g., Collinge et al. 2005). The lack of red UV spectra in WLQs may also be reflected by the upper limit we place on the mean column density of neutral absorption in these sources (§ 3.3; Table 4). This is broadly consistent with the idea that the weakness of the emission lines is not a consequence of dust absorption, even though the upper limit on N_H does not provide a tight constraint on allowed reddening in the rest-frame UV.

Another indication that WLQs are related to typical quasars lies in their α_{ox} distribution (with a spread of ~ 0.6 for the radio-quiet sources; see Fig. 5). We tested whether this α_{ox} distribution is consistent with the optically selected sample of Gibson et al. (2008), that includes SDSS quasars with *Chandra* detections. We performed a KS test and found that the α_{ox} distributions were consistent between 139 radio-quiet, non-BAL quasars from sample B of Gibson et al. (2008) and our seven radio-quiet WLQs. We found that the null hypothesis, that the two samples were drawn from the same parent distribution, cannot be rejected with a confidence level of 97.3%. After scaling out the dependence of α_{ox} on optical luminosity (§ 3), we also performed a KS test on the two $\Delta\alpha_{ox}$ distributions of these samples and found that the null hypothesis cannot be rejected with a confidence level of 94.8%.

As noted in S06, at least two sources at low redshift, PG 1407+265 at $z = 0.94$ (McDowell et al. 1995) and PHL 1811 at $z = 0.19$ (Leighly et al. 2007b), lack high-ionization emission lines in their UV spectra (although some low-ionization lines are detected in both sources). An additional source, 2QZ J215454.3–305654 at $z = 0.494$ (Londish et al. 2004), may also be related to these two, as it shows only an [O III] $\lambda 5007$ emission line; however, since UV spectroscopy has not yet been performed, it is unknown whether it displays higher ionization lines. These three sources, which also appear different from BL Lacs, may perhaps be the low-redshift analogs of the $z \gtrsim 2.2$ WLQs; they are plotted separately in Figure 5. The fact that all our WLQs lie at high

redshifts is clearly a selection effect due to the requirement of a Lyman break detection. We therefore expect that WLQs should exist also at lower redshifts.

Figure 7 shows a comparison between the UV spectrum of one of these low-redshift WLQs, PHL 1811, and the mean UV spectrum of ten of our high-redshift WLQs (i.e., excluding the Keck spectrum of SDSS J1335+3533) alongside the mean UV spectrum of ‘typical’ SDSS quasars. Overall, the mean spectrum of our high-redshift WLQs appears similar to the spectrum of PHL 1811, and the high-ionization emission lines in both spectra are significantly weaker compared to the mean SDSS spectrum. The Ly α +N V complex in PHL 1811 has $EW = 24 \text{ \AA}$, which is somewhat larger than our definition of WLQs ($EW < 10 \text{ \AA}$), but the C IV emission line in that source is exceptionally weak with $EW = 6.6 \text{ \AA}$ (Leighly et al. 2007b). A comprehensive comparison between our high-redshift WLQs and their putative low-redshift counterparts requires rest-frame optical spectroscopy of our sources to search for low-ionization emission lines.

Weak emission lines in AGNs are typically associated with high luminosities in what has been termed the ‘Baldwin effect’, i.e., the anticorrelation between emission-line EW and quasar luminosity (where the anticorrelation is stronger and steeper for emission lines with higher ionization potentials; e.g., Baldwin 1977; Dietrich et al. 2002). In this context, WLQs might have been expected to dominate the high-luminosity end of the quasar luminosity function, but this is certainly not the case (e.g., Just et al. 2007 studied the properties of the 32 most luminous quasars in SDSS DR3; this sample does not include a single WLQ).

A different interpretation of the Baldwin effect has been suggested by Baskin & Laor (2004), who have shown that $EW(C\text{ IV})$ depends more strongly on the normalized accretion rate (i.e., L/L_{Edd} , where L is the AGN bolometric luminosity) than on L_{UV} in a sample of 81 low–moderate luminosity AGNs (i.e., with $L \sim 10^{43}–10^{46} \text{ ergs s}^{-1}$) from Boroson & Green (1992). Using virial black-hole masses measured from the SDSS spectra of ~ 60000 quasars, Shen et al. (2008) have shown that L/L_{Edd} exhibits a lognormal distribution (clearly, WLQs could not have been included in their analysis due to their lack of emission lines). Can this be related to the result of Diamond-Stanic et al. (2009) who found that $EW(\text{Ly}\alpha + \text{N V})$ values in SDSS quasars also exhibit a lognormal distribution (§ 1)? In this scenario, WLQs may constitute a significant deviation from the L/L_{Edd} distribution at the high- L/L_{Edd} end, in analogy with their significant deviation from the EW distribution at the low-EW end. Testing this idea and the hypothesis that emission-line EW is correlated primarily with L/L_{Edd} across the entire AGN luminosity range requires extending the Baskin & Laor (2004) analysis to much higher luminosities, such as those of our WLQs; this is beyond the scope of this work. Near-IR spectroscopy of the Mg II and H β spectral regions in WLQs is required to determine L/L_{Edd} values in these sources directly, provided these lines are sufficiently strong to measure (e.g., Shemmer et al. 2004). A high accretion rate has also been proposed for at least one of the low-redshift WLQs, PHL 1811, to explain the absence of the high-ionization emission lines (Leighly et al. 2007b).

If WLQs are AGNs that constitute the high-end tail of the L/L_{Edd} distribution, then they may also be expected to exhibit steep hard-X-ray continua (see, e.g., Brandt et al. 1997; Shemmer et al. 2008). For example, high-quality *XMM-Newton* spectra of two of the low-redshift WLQs,

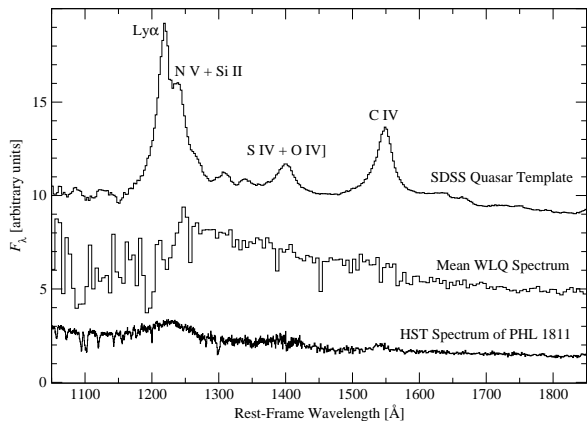


FIG. 7.— A comparison between the mean UV spectrum of ~ 2000 SDSS quasars (*top*; Vanden Berk et al. 2001), the mean UV spectrum of ten of our WLQs with SDSS spectra (*middle*; see also Fig. 1), and the *HST/STIS* UV spectrum of PHL 1811 (*bottom*; Leighly et al. 2007b). All spectra are scaled arbitrarily in flux for clarity. Prominent emission lines are marked on the mean SDSS spectrum.

PG 1407+265 and PHL 1811, indeed show relatively steep X-ray continua at rest-frame energies $\gtrsim 2$ keV, with photon indices of $\Gamma = 2.19 \pm 0.07$ (Piconcelli et al. 2005) and $\Gamma = 2.28^{+0.12}_{-0.11}$ (Leighly et al. 2007a), respectively. High-quality X-ray spectra of high-redshift WLQs have not yet been obtained to test whether they show similar X-ray spectral properties. The X-ray brightest source in our sample, SDSS J1231+0138, had only 110 counts, but it does not exhibit an unusually steep hard-X-ray power-law spectrum ($\Gamma = 1.76^{+0.35}_{-0.34}$, § 3.2). However, this WLQ is also the radio-brightest source in our sample (involving perhaps jet-related emission contributing to its X-ray spectrum). We had already pointed out that our joint spectral fitting of a sample of WLQs does not provide any evidence or hint of a steep hard-X-ray spectrum (§ 3.3; Table 4). Moreover, if we consider WLQs to have $L/L_{\text{Edd}} \gtrsim 1$ (i.e., at the extreme high end of the Shen et al. 2008 L/L_{Edd} distribution), then following the Γ - L/L_{Edd} correlation of Shemmer et al. (2008) these sources should have hard-X-ray slopes with $\Gamma \gtrsim 2.5$. Such steep slopes are rejected with $>99.9\%$ confidence from our joint spectral fits. Interestingly, however, Table 2 may hint that at least two WLQs, SDSS J0317–0758 and SDSS J0928+1848 (with insufficient counts for a proper spectral analysis), may have steep hard X-ray spectra, based on the effective photon indices obtained from their band ratios. Future *XMM-Newton* spectroscopic observations of these as well as a statistically representative sample of WLQs are required for a robust test of this idea. Such observations may also provide better constraints on putative Compton reflections in these sources.

5. SUMMARY

We present new *Chandra* observations of nine high-redshift quasars with weak or undetectable high-ionization emission lines in their UV spectra (WLQs). Adding archival X-ray observations of six additional sources of this class has enabled us to place the strongest constraints yet on the X-ray properties of 15 sources of this rare class of AGNs. All but two of these 15 sources are X-ray detected, and for the strongest X-ray (and radio) source we have determined a power-law photon

index of $\Gamma = 1.76^{+0.35}_{-0.34}$ in the rest-frame $\sim 2 - 35$ keV spectral band. A joint spectral fit of the X-ray spectrum of 11 of these sources gives an upper limit on the mean intrinsic neutral absorption column density of $N_{\text{H}} \lesssim 5 \times 10^{22} \text{ cm}^{-2}$; the corresponding mean power-law photon index is $\Gamma = 1.79^{+0.17}_{-0.16}$. These results provide further support to the idea that the weakness of the UV lines is not a consequence of dust absorption, and they show that the mean hard-X-ray spectral slope of WLQs is consistent with the spectral slopes observed in typical radio-quiet quasars.

Our new X-ray information on high-redshift WLQs has brought us one step closer to distinguishing between two competing models for their nature. Although a boosted-continuum interpretation for the missing emission lines cannot be ruled out based on our current data, we find that WLQs occupy an almost distinct region of the X-ray-radio parameter space from BL Lacs. WLQs are mostly X-ray and radio weak compared to lower-redshift BL Lacs. The strongest argument against the association of WLQs with BL Lacs is the lack of a parent population of X-ray- and radio-bright sources at high redshift. We discuss additional observations that are required to test whether WLQs are quasars with extreme properties. A key goal is to check whether WLQs are quasars with extremely high accretion rates; our current constraints on the mean Γ for these sources do not support this idea. Such efforts should provide a better understanding not only of WLQs and the BL Lac phenomena, but of the AGN population as a whole.

We gratefully acknowledge the financial support of *Chandra* X-ray Center grant G07-8101X, NASA LTSA grant NAG5-13035 (O. S., W. N. B., D. P. S.), and NSF grant AST-0702766 (M. A. S.). We thank Annalisa Celotti, Abe Falcone, and Eric Perlmutter for fruitful discussions. We also thank an anonymous referee for a thoughtful report that assisted in improving the presentation of this work. Funding for the SDSS and SDSS-II has been provided by the Alfred P. Sloan Foundation, the Participating Institutions, the National Science Foundation, the U.S. Department of Energy, the National Aeronautics and Space Administration, the Japanese Monbukagakusho, the Max Planck Society, and the Higher Education Funding Council for England. The SDSS Web Site is <http://www.sdss.org/>. The SDSS is managed by the Astrophysical Research Consortium for the Participating Institutions. The Participating Institutions are the American Museum of Natural History, Astrophysical Institute Potsdam, University of Basel, University of Cambridge, Case Western Reserve University, University of Chicago, Drexel University, Fermilab, the Institute for Advanced Study, the Japan Participation Group, Johns Hopkins University, the Joint Institute for Nuclear Astrophysics, the Kavli Institute for Particle Astrophysics and Cosmology, the Korean Scientist Group, the Chinese Academy of Sciences (LAMOST), Los Alamos National Laboratory, the Max-Planck-Institute for Astronomy (MPIA), the Max-Planck-Institute for Astrophysics (MPA), New Mexico State University, Ohio State University, University of Pittsburgh, University of Portsmouth, Princeton University, the United States Naval Observatory, and the University of Washington. This research has made use of the NASA/IPAC Extragalactic Database (NED) which is operated by the Jet Propulsion Laboratory, California Institute of Technology, under contract with the National Aeronautics and Space Administration.

REFERENCES

- Anderson, S. F., et al. 2001, *AJ*, 122, 503
 Anderson, S. F., et al. 2007, *AJ*, 133, 313
 Arnaud, K. A. 1996, *ASP Conf. Ser.* 101: *Astronomical Data Analysis Software and Systems V*, 101, 17
 Avni, Y. 1976, *ApJ*, 210, 642
 Baldwin, J. A. 1977, *ApJ*, 214, 679
 Baskin, A., & Laor, A. 2004, *MNRAS*, 350, L31
 Becker, R. H., White, R. L., & Helfand, D. J. 1995, *ApJ*, 450, 559
 Bianchi, S., Guainazzi, M., Matt, G., & Fonseca Bonilla, N. 2007, *A&A*, 467, L19
 Boroson, T. A., & Green, R. F. 1992, *ApJS*, 80, 109
 Brandt, W. N., Mathur, S., & Elvis, M. 1997, *MNRAS*, 285, L25
 Cash, W. 1979, *ApJ*, 228, 939
 Collinge, M. J., et al. 2005, *AJ*, 129, 2542
 Condon, J. J., Cotton, W. D., Greisen, E. W., Yin, Q. F., Perley, R. A., Taylor, G. B., & Broderick, J. J. 1998, *AJ*, 115, 1693
 Diamond-Stanic, A., et al. 2009, *ApJ*, submitted
 Dickey, J. M., & Lockman, F. J. 1990, *ARA&A*, 28, 215
 Dietrich, M., Hamann, F., Shields, J. C., Constantin, A., Vestergaard, M., Chaffee, F., Foltz, C. B., & Junkkarinen, V. T. 2002, *ApJ*, 581, 912
 Eadie, W. T., Dryard, D., James, F. E., Roos, M., & Sadoulet, B. 1971, *Statistical Methods in Experimental Physics*, (Amsterdam: North-Holland)
 Fan, X., et al. 1999, *ApJ*, 526, L57
 Fan, X., et al. 2001, *AJ*, 121, 31
 Fan, X., et al. 2006, *AJ*, 131, 1203
 Freeman, P. E., Kashyap, V., Rosner, R., & Lamb, D. Q. 2002, *ApJS*, 138, 185
 Garmire, G. P., Bautz, M. W., Ford, P. G., Nousek, J. A., & Ricker, G. R. 2003, *Proc. SPIE*, 4851, 28
 Gehrels, N. 1986, *ApJ*, 303, 336
 Gibson, R. R., Brandt, W. N., & Schneider, D. P. 2008, *ApJ*, 685, 773
 Iwasawa, K., & Taniguchi, Y. 1993, *ApJ*, 413, L15
 Jiang, L., Fan, X., Ivezić, Ž., Richards, G. T., Schneider, D. P., Strauss, M. A., & Kelly, B. C. 2007, *ApJ*, 656, 680
 Kellermann, K. I., Sramek, R., Schmidt, M., Shaffer, D. B., & Green, R. 1989, *AJ*, 98, 1195
 Kraft, R. P., Burrows, D. N., & Nousek, J. A. 1991, *ApJ*, 374, 344
 Landt, H., Padovani, P., Perlman, E. S., Giommi, P., Bignall, H., & Tzioumis, A. 2001, *MNRAS*, 323, 757
 Laurent-Muehleisen, S. A., Kollgaard, R. I., Feigelson, E. D., Brinkmann, W., & Siebert, J. 1999, *ApJ*, 525, 127
 Leighly, K. M., Halpern, J. P., Jenkins, E. B., Grupe, D., Choi, J., & Prescott, K. B. 2007a, *ApJ*, 663, 103
 Leighly, K. M., Halpern, J. P., Jenkins, E. B., & Casebeer, D. 2007b, *ApJS*, 173, 1
 Londish, D., Heidt, J., Boyle, B. J., Croom, S. M., & Kedziora-Chudczer, L. 2004, *MNRAS*, 352, 903
 Lyons, L. 1991, *Data Analysis for Physical Science Students* (Cambridge: Cambridge Univ. Press)
 McDowell, J. C., Canizares, C., Elvis, M., Lawrence, A., Markoff, S., Mathur, S., & Wilkes, B. J. 1995, *ApJ*, 450, 585
 Oke, J. B., & Gunn, J. E. 1983, *ApJ*, 266, 713
 Padovani, P., Giommi, P., Landt, H., & Perlman, E. S. 2007, *ApJ*, 662, 182
 Page, K. L., Reeves, J. N., O'Brien, P. T., & Turner, M. J. L. 2005, *MNRAS*, 364, 195
 Perlman, E. S., et al. 1996, *ApJS*, 104, 251
 Perlman, E. S., Padovani, P., Giommi, P., Sambruna, R., Jones, L. R., Tzioumis, A., & Reynolds, J. 1998, *AJ*, 115, 1253
 Perlman, E. S., Padovani, P., Landt, H., Stocke, J. T., Costamante, L., Rector, T., Giommi, P., & Schachter, J. F. 2001, *ASP Conf. Ser.* 227: *Blazar Demographics and Physics*, 227, 200
 Piconcelli, E., et al. 2005, *A&A*, 432, 15
 Pier, J. R., Munn, J. A., Hindsley, R. B., Hennessy, G. S., Kent, S. M., Lupton, R. H., & Ivezić, Ž. 2003, *AJ*, 125, 1559
 Plotkin, R. M., Anderson, S. F., Hall, P. B., Margon, B., Voges, W., Schneider, D. P., Stinson, G., & York, D. G. 2008, *AJ*, 135, 2453
 Rector, T. A., Stocke, J. T., Perlman, E. S., Morris, S. L., & Gioia, I. M. 2000, *AJ*, 120, 1626
 Reeves, J. N., & Turner, M. J. L. 2000, *MNRAS*, 316, 234
 Richards, G. T., et al. 2002, *AJ*, 123, 2945
 Sambruna, R. M., Maraschi, L., & Urry, C. M. 1996, *ApJ*, 463, 444
 Schlegel, D. J., Finkbeiner, D. P., & Davis, M. 1998, *ApJ*, 500, 525
 Schneider, D. P., et al. 2001, *AJ*, 121, 1232
 Schneider, D. P., et al. 2003, *AJ*, 126, 2579
 Schneider, D. P., et al. 2005, *AJ*, 130, 367
 Schneider, D. P., et al. 2007, *AJ*, 134, 102
 Shemmer, O., Netzer, H., Maiolino, R., Oliva, E., Croom, S., Corbett, E., & di Fabrizio, L. 2004, *ApJ*, 614, 547
 Shemmer, O., et al. 2006, *ApJ*, 644, 86 (S06)
 Shemmer, O., Brandt, W. N., Netzer, H., Maiolino, R., & Kaspi, S. 2008, *ApJ*, 682, 81
 Shen, Y., Greene, J. E., Strauss, M. A., Richards, G. T., & Schneider, D. P. 2008, *ApJ*, 680, 169
 Steffen, A. T., Strateva, I., Brandt, W. N., Alexander, D. M., Koekemoer, A. M., Lehmer, B. D., Schneider, D. P., & Vignali, C. 2006, *AJ*, 131, 2826
 Stickel, M., Fried, J. W., Kuehr, H., Padovani, P., & Urry, C. M. 1991, *ApJ*, 374, 431
 Stocke, J. T., & Perrenod, S. C. 1981, *ApJ*, 245, 375
 Stocke, J. T. 2001, *Blazar Demographics and Physics*, 227, 184
 Urry, C. M., & Padovani, P. 1995, *PASP*, 107, 803
 Vanden Berk, D. E., et al. 2001, *AJ*, 122, 549
 Vignali, C., Brandt, W. N., Schneider, D. P., & Kaspi, S. 2005, *AJ*, 129, 2519
 York, D. G., et al. 2000, *AJ*, 120, 1579
 Zhou, X.-L., & Wang, J.-M. 2005, *ApJ*, 618, L83

TABLE 3
X-RAY, OPTICAL, AND RADIO PROPERTIES

Object (SDSS J)	N_{H}^{a}	AB_{1450}	M_B	$f_{2500 \text{ \AA}}^{\text{b}}$	$\log(\nu L_{\nu})$ 2500 \AA	Count Rate ^c	f_x^{d}	$f_2 \text{ keV}^{\text{e}}$	$\log(\nu L_{\nu})$ 2 keV	$\log L$ 2–10 keV	α_{ox}	$\Delta\alpha_{\text{ox}} (\sigma)^{\text{f}}$	$\alpha_{\text{ro}}^{\text{g}}$
(1)	(2)	(3)	(4)	(5)	(6)	(7)	(8)	(9)	(10)	(11)	(12)	(13)	(14)
031712.23–075850.3	5.14	18.7	–27.1	15.8	46.5	$5.40^{+1.35}_{-1.10}$	$22.1^{+5.5}_{-4.5}$	12.19	45.0	45.2	–1.58	+0.12 (0.8)	> –0.23 ^l
092832.90+184824.4	3.83	17.4	–28.9	52.1	47.2	$13.13^{+2.08}_{-1.81}$	$51.7^{+8.2}_{-7.1}$	37.03	45.7	45.9	–1.59	+0.21 (1.6)	–0.24
101204.04+531331.8 ^h	0.78	19.3	–26.6	9.2	46.3	$3.28^{+4.85}_{-1.86}$ ^k	$20.8^{+30.7}_{-11.8}$	12.37	45.1	45.3	–1.49	+0.18 (1.3)	–0.28
114153.34+021924.3	2.30	18.5	–27.6	18.4	46.7	$7.18^{+1.61}_{-1.33}$	$27.1^{+6.1}_{-5.0}$	18.07	45.3	45.5	–1.54	+0.19 (1.3)	–0.24
121221.56+534128.0	1.71	18.6	–27.3	17.2	46.6	$0.73^{+0.71}_{-0.39}$	$2.7^{+2.6}_{-1.5}$	1.65	44.2	44.4	–1.93	–0.21 (1.5)	> –0.08
123132.38+013814.0	1.81	18.6	–27.4	17.5	46.7	$20.44^{+2.39}_{-2.23}$	$76.0^{+9.3}_{-8.3}$	47.94	45.7	45.9	–1.37	+0.35 (2.4)	–0.32
123743.08+630144.9 ^h	1.66	19.0	–27.1	12.0	46.5	< 3.30 ^k	< 16.6	< 10.88	< 45.1	< 45.3	< –1.55	< +0.15 (< 1.0)	> –0.12
130216.13+003032.1 ⁱ	1.57	19.5	–27.0	7.3	46.5	$0.09^{+0.12}_{-0.06}$	$0.3^{+0.5}_{-0.2}$	0.28	43.7	43.9	–2.08	–0.38 (2.6)	> –0.16
133422.63+475033.6	1.63	19.1	–27.6	10.7	46.7	$1.19^{+0.41}_{-0.32}$	$4.4^{+1.5}_{-1.2}$	3.90	44.9	45.1	–1.70	+0.02 (0.2)	> –0.13
133550.81+353315.8	0.92	19.8 ⁱ	–27.3	5.8	46.6	$0.13^{+0.13}_{-0.07}$	$0.5^{+0.5}_{-0.3}$	0.48	44.1	44.3	–1.95	–0.24 (1.7)	> –0.18
142103.83+343332.0	1.16	19.0	–27.8	12.5	46.8	$0.16^{+0.21}_{-0.10}$	$0.6^{+0.8}_{-0.4}$	0.50	44.0	44.2	–2.07	–0.33 (2.3)	> –0.11

^a Neutral Galactic absorption column density in units of 10^{20} cm^{-2} taken from Dickey & Lockman (1990).

^b Flux density at rest-frame 2500 \AA in units of $10^{-28} \text{ erg cm}^{-2} \text{ s}^{-1} \text{ Hz}^{-1}$.

^c Observed count rate computed in the 0.5–2 keV band in units of $10^{-3} \text{ counts s}^{-1}$.

^d Galactic absorption-corrected flux in the observed 0.5–2 keV band in units of $10^{-15} \text{ erg cm}^{-2} \text{ s}^{-1}$.

^e Flux density at rest-frame 2 keV in units of $10^{-32} \text{ erg cm}^{-2} \text{ s}^{-1} \text{ Hz}^{-1}$.

^f The difference between measured and predicted α_{ox} ($\Delta\alpha_{\text{ox}}$), and the significance of that difference (σ), based on the Just et al. (2007) $\alpha_{\text{ox}}-L_V(2500 \text{ \AA})$ relation.

^g Unless otherwise noted, radio-to-optical flux ratios (α_{ro} ; see § 3.1 for the conversion of these values to the radio-loudness parameter R) involve radio flux densities at an observed-frame frequency of 1.4 GHz taken from the FIRST survey (Becker et al. 1995); upper limits on α_{ro} are calculated from the 3 σ FIRST detection threshold at the source position.

^h X-ray data obtained from serendipitous *XMM-Newton* observations.

ⁱ The X-ray count rate, fluxes, luminosities, and α_{ox} were obtained from the merged event file of two *Chandra* exposures (see § 2).

^j Obtained from the Keck spectrum of Fan et al. (2006).

^k Count rate corrected for the exposure map.

^l Flux density at an observed-frame frequency of 1.4 GHz taken from the NVSS survey (Condon et al. 1998); upper limits are calculated from the NVSS detection threshold of 2.5 mJy.

TABLE 5
X-RAY, OPTICAL, AND RADIO PROPERTIES OF THE BL LAC SAMPLE

BL Lac	RA (J2000)	DEC (J2000)	z	$\log[\nu L_\nu(2 \text{ keV})]$ (ergs s $^{-1}$)	$\log[\nu L_\nu(5500 \text{ \AA})]$ (ergs s $^{-1}$)	$\log[\nu L_\nu(5 \text{ GHz})]$ (ergs s $^{-1}$)	α_{ox}	α_{ro}	Reference
SDSS J000157.23–103117.3	0.48850	–10.52148	0.252	≤ 43.30	44.05	41.53	≤ -1.35	–0.50	1
RGB J0007+472	2.00000	47.20222	0.280	43.95	44.33	41.81	–1.21	–0.50	2
SDSS J001736.91+145101.9	4.40378	14.85053	0.303	≤ 44.09	44.70	42.03	≤ -1.30	–0.47	3
SDSS J002200.95+000657.9	5.50396	0.11610	0.306	44.24	44.03	40.42	–0.99	–0.30	1
WGA J0032.5–2849	8.13792	–28.82222	0.324	43.68	44.06	42.34	–1.21	–0.65	4
WGA J0043.3–2638	10.84417	–26.65139	0.451	44.12	45.02	42.40	–1.41	–0.48	4
SDSS J005620.07–093629.7	14.08366	–9.60826	0.103	43.80	43.90	41.22	–1.10	–0.47	1
WGA J0100.1–3337	15.03917	–33.62556	0.875	43.97	44.59	43.24	–1.30	–0.72	4
SDSS J010326.01+152624.8	15.85839	15.44021	0.246	≤ 43.81	44.43	42.42	≤ -1.30	–0.59	3
RGB J0110+418	17.52000	41.83083	0.096	43.23	43.47	40.28	–1.16	–0.38	2

REFERENCES. — (1) Plotkin et al. (2008); (2) Laurent-Muehleisen et al. (1999); (3) Collinge et al. (2005); (4) Perlman et al. (1998).

NOTE. — The full version of this table is available in the electronic edition online. Luminosities, α_{ox} , and α_{ro} were computed from the data given in the references (last column) using the K -corrections outlined in § 4.1.